

Herschel's view into Mira's head[★]

A. Mayer¹, A. Jorissen², F. Kerschbaum¹, S. Mohamed³, S. Van Eck², R. Ottensamer¹, J.A.D.L. Blommaert⁴, L. Decin⁴, M.A.T. Groenewegen⁵, Th. Posch¹, B. Vandenbussche⁴, and Ch. Waelkens⁴

¹ University of Vienna, Department of Astronomy, Türkenschanzstraße 17, A-1180 Wien, Austria
e-mail: a.mayer@univie.ac.at

² Institut d'Astronomie et d'Astrophysique, Université Libre de Bruxelles, CP. 226, Boulevard du Triomphe, B-1050 Brussels, Belgium

³ Argelander-Institut für Astronomie, Universität Bonn, Auf dem Hügel 71, D-53121 Bonn, Germany

⁴ Instituut voor Sterrenkunde, K.U. Leuven, Celestijnenlaan, 200D, B-3001 Leuven, Belgium

⁵ Koninklijke Sterrenwacht van België, Ringlaan 3, B-1180 Brussels, Belgium

Received ...; accepted ...

ABSTRACT

Herschel's PACS instrument observed the environment of the binary system Mira Ceti in the 70 and 160 μm bands. These images reveal bright structures shaped as five broken arcs and fainter filaments in the ejected material of Mira's primary star, the famous AGB star *o* Ceti. The overall shape of the IR emission around Mira deviates significantly from the expected alignment with Mira's exceptionally high space velocity. The observed broken arcs are neither connected to each other nor are they of a circular shape; they stretch over angular ranges of 80 to 100 degrees. By comparing Herschel and GALEX data, we found evidence for the disruption of the IR arcs by the fast outflow visible in both $H\alpha$ and the far UV. Radial intensity profiles are derived, which place the arcs at distances of 6–85'' (550 – 8000 AU) from the binary. Mira's IR environment appears to be shaped by the complex interaction of Mira's wind with its companion, the bipolar jet, and the ISM.

Key words. Stars: oxygen – Stars: asymptotic giant branch – Stars: Mass loss – Stars: Binarity – Infrared: stars – Interstellar medium

1. Introduction

Centuries ago *o* Ceti confused the astronomers all over the world with its appearance and disappearance on the night sky and was therefore named *Mira*, the wonderful, by Hevelius (1662).

Today we know that Mira is a wind-accreting binary star system (Reimers & Cassatella 1985) at a distance of 91.7 pc (corresponding to a parallax of 10.9 ± 1.2 mas; van Leeuwen 2007) consisting of the primary star Mira A (*o* Ceti) and its companion Mira B (VZ Ceti). Mira A is an M-type oxygen-rich star with a pulsation period of 331 d and a brightness amplitude in the visible of 8 mag. Moreover, Mira A is the prototype of stars in their late stage of evolution residing on the asymptotic giant branch (AGB). The nature of Mira B has been unknown for long; with an effective temperature of about 10 000 K, it might either be a main-sequence star or a white dwarf (Karovska et al. 1997), but recent observations show strong evidence in favour of a white dwarf (Sokoloski & Bildsten 2010). From a Hubble Space Telescope observation, Karovska et al. (1997) found the separation of Mira AB to be $\approx 0.6''$, which corresponds to 55 AU. A very uncertain orbit, based on astrometric measurements since 1923, which has a period of ≈ 500 yr, has been published by Prieur et al. (2002).

Stars on the AGB loose a significant fraction of their mass in the form of a stellar wind. For Mira A, a moderate mass loss rate of $10^{-7} M_{\odot} \text{ yr}^{-1}$ was determined by Maun & Caux (1992), which corresponds to a dust mass-loss rate of about $5.5 \times 10^{-10} M_{\odot} \text{ yr}^{-1}$ (Meixner, 2011, priv. comm.). From mm-CO lines, Josselin et al.

(2000) found a wind expansion velocity of 4 km s^{-1} and a molecular envelope around the binary system with a size of about $20''$. This envelope is disrupted by a slow bipolar outflow of about 8 km s^{-1} (Josselin et al. 2000), but a high-velocity component at 160 km s^{-1} has been observed by Meaburn et al. (2009). In the outer environment of Mira, a spectacular observation with the GALEX ultraviolet satellite (Martin et al. 2007) revealed a cometary-like structure with an extension of more than 2° ($\approx 4 \text{ pc}$) from head to tail. Martin et al. (2007) attribute this tail to Mira's exceptionally high space velocity of $\approx 110 \text{ km s}^{-1}$ and the resulting strong interaction of the stellar wind with the interstellar medium (ISM). This structure was also observed in the 21 cm H I line (Matthews et al. 2008) and is well reproduced by the hydrodynamic simulations of Wareing et al. (2007), Raga & Cantó (2008) and Esquivel et al. (2010). In the vicinity of the binary system, knot-shaped enhancements of the UV and $H\alpha$ emission were found at a distance of $1'$ to $2'$ from the binary (Martin et al. 2007; Meaburn et al. 2009), corresponding to 5500 to 11 000 AU, and in a direction consistent with that of the bipolar outflow observed by Josselin et al. (2000). In the far IR Ueta (2008) resolved with the Spitzer Space Telescope the contours of Mira's astropause including the circumbinary envelope, termination shock, and astrosheath.

The present study offers a detailed view of Mira's circumstellar shell(s) thanks to the high spatial resolution of the PACS instrument (which has a point-spread function of $5''.6$ full-width at half-maximum at $70 \mu\text{m}$) onboard the Herschel satellite. The images presented here reveal clumpy broken arcs (see Sect. 3.1) that result from the complex interactions of the wind with the ISM, the companion and the fast outflow.

[★] Herschel is an ESA space observatory with science instruments provided by European-led Principal Investigator consortia and with important participation from NASA.

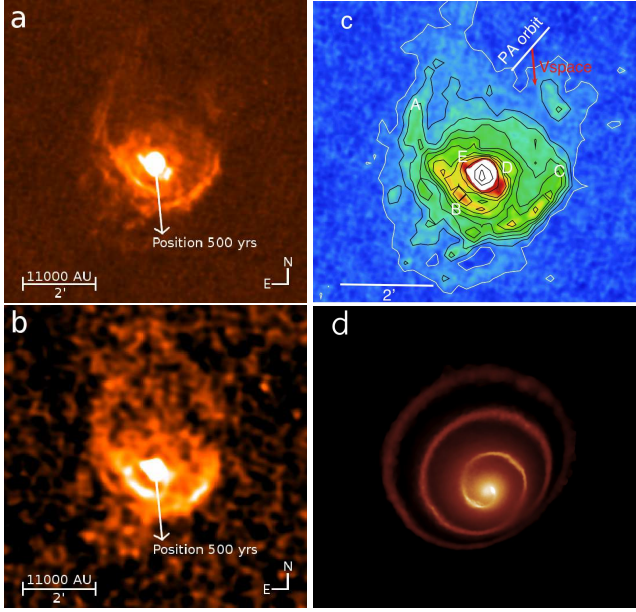


Fig. 1. Panel (a): deconvolved PACS image at $70\ \mu\text{m}$. The arrow indicates the space motion and the position in 500 yrs; (b) is the same for the $160\ \mu\text{m}$ band and (c) is the $70\ \mu\text{m}$ deconvolved PACS image with contours and arcs labelled as A, B, C, D and E. The lowest contour is the 3σ threshold (and is depicted in white), the arrow labelled with V_{space} shows the direction of the space motion, the bar labelled PA orbit gives the orientation of the major axis of the apparent orbit, orthogonal to the node line. Panel (d) results from the ‘toy model’ described in Sect. 3.3 that is based on the hydrodynamical simulations of Mohamed & Podsiadlowski (2007, 2011).

Table 1. Kinematic data for Mira. Negative inclinations are towards the observer. The various vectors are displayed in a 3D view in Fig. 4. The adopted solar motion to convert heliocentric velocities in LSR velocities is $(U, V, W)_{\odot} = (11.10, 12.24, 7.25)\ \text{km s}^{-1}$ (Schönrich et al. 2010). The matrix to convert equatorial velocities into galactic velocities is taken from Johnson & Soderblom (1987).

$b(^{\circ})$	-58	ϖ (mas)	10.9 ± 1.2^a
$\mu_{\alpha, \text{LSR}}$ (mas yr $^{-1}$)	-20.93 ^a	$\mu_{\delta, \text{LSR}}$ (mas yr $^{-1}$)	-222.39 ^a
RV_{LSR} (km s $^{-1}$)	47.2 ^f	$V_{\text{space, LSR}}$ (km s $^{-1}$)	107.9
$V_{\text{space, LSR}}$ P.A. ($^{\circ}$)	185.4	$V_{\text{space, LSR}}$ i ($^{\circ}$)	25.9
V_{wind} (km s $^{-1}$)	4 ^c	V_{outflow} (km s $^{-1}$)	160 ± 10^d
Bipolar flow PA ($^{\circ}$)	168-180 ^d	Bipolar flow i ($^{\circ}$)	-69 ^d
Orbital pole PA ($^{\circ}$)	228 ^e	Orbital pole i ($^{\circ}$)	$\pm 22^e$
P (yr)	$\approx 500^e$	a (AU)	$\approx 100^{a,e}$
$M_1 + M_2$ (M_{\odot})	4.4 ^e	\dot{M} ($M_{\odot}\ \text{yr}^{-1}$)	$10^{-7\ b}$

a: van Leeuwen (2007); b: Maun & Caux (1992); c: Josselin et al. (2000); d: Martin et al. (2007); Meaburn et al. (2009); e: Prieur et al. (2002); f: Fong et al. (2006)

2. Observations and data reduction

The observations of Mira took place on February 9, 2010, using the PhotoArray Camera and Spectrometer (PACS; Poglitsch et al. 2010) onboard Herschel as part of the MESS (Mass-loss of Evolved StarS) Guaranteed Time Key Program (Groenewegen et al. 2011).

The PACS camera observed at $70\ \mu\text{m}$ and $160\ \mu\text{m}$ simultaneously, covering a field of $30' \times 30'$ on the sky with a scan-map mode. For the basic data pro-

cessing to produce the images displayed in Fig. 1, the Herschel Interactive Processing Environment (HIPE) was used (Ardila & Science Ground Segment Consortium 2010) together with Scanamorphos, an IDL software for building scan maps from PACS (and SPIRE) observations (Roussel 2011). Finally, we deconvolved the images as described by Ottensamer et al. (2011). Although the PACS instrument offers a resolution of $3.2''$ per pixel in the $70\ \mu\text{m}$ (blue) band and $6.4''$ per pixel at $160\ \mu\text{m}$ (red band), the images shown in Fig. 1 are oversampled by a factor 3.2, resulting in a sampling of $1''$ and $2''$ per pixel (at 70 and $160\ \mu\text{m}$, respectively), to be compared with the FWHM of $5''.6$ and $11''.4$ at those wavelengths. We estimate the average background emission to be $1.5 \times 10^{-4}\ \text{Jy pixel}^{-1}$ in the blue and $3 \times 10^{-4}\ \text{Jy pixel}^{-1}$ in the red band, yielding the 1σ sensitivity.

3. Results and discussion

3.1. IR images

Mira's environment is remarkably structured and exhibits arc-like structures in the surrounding of the binary system, labelled A to E in Fig. 1c. The best-defined and brightest arc, C, stretches over position angles (PAs) $\sim 190^{\circ} - 270^{\circ}$ (south-west to west), is well detached from the star and covers a range of angular separation from $67''$ (6100 AU) at the closest point to $85''$ (7800 AU) at the most distant point from the star. The intensity was integrated over this PA range and the resulting radial intensity profile (Fig. 2) clearly shows the arc as a plateau in the diagram. The extension of this plateau confirms that the arc is non-circular or, if circular, is not centred on the position of the star. We found another arc, D, in the same direction as arc C but much closer to the star and stretching over much smaller PAs. In the radial intensity profile, arc D is visible as a bump located at a distance of $21 - 28''$ (1900–2600 AU). East of Mira more arcs are visible. In the south-east direction, we see arc B close to the star. It stretches over PAs 75° to 180° and is more circular than arc C and therefore appears as a narrow peak in the radial intensity profile at a distance of $41''$ (3800 AU) from the binary (Fig. 2).

Farther out, directly to the east, we find another structure, arc A, stretching towards north-east. In the integrated intensity profile, it can be recognized as a small plateau representing its fairly faint nature at a distance of $68 - 89''$ (6200–8200 AU). This matches the distance of arc C, which leads to the suggestion that both arcs are somehow related to each other.

It is also possible that another arc, E, is present in the south-east direction, very close to the binary at a distance of less than $15''$ (1400 AU), of which we only see the edge at a PA of about 65° . It is noteworthy that the arc sequence E-D-B-C-A is a sequence of both increasing distance from the star and increasing PA range, arc E being the shortest and closest to the star, and A the longest and farthest.

The overall 3σ emission above the $70\ \mu\text{m}$ IR background of Mira, visible in Fig. 1c as the outermost contour, spans as far as $157''$ towards the south-east. It is remarkable that the extension of the emission is towards a position angle of $\approx 160^{\circ}$ because one would expect the emission to be aligned with Mira's space motion, but that motion is in the direction of PA = 185° . In Fig. 1c we also indicated the orientation of the major axis of the apparent orbit, which is oriented along a PA of $\approx 140^{\circ}$ (Prieur et al. 2002). As discussed in more detail in Sect. 3.3, the orbital motion and the mass transfer from the binary can also shape its environment. Nevertheless, the extension of the IR emission lies between both values and makes a distinct attribution difficult.

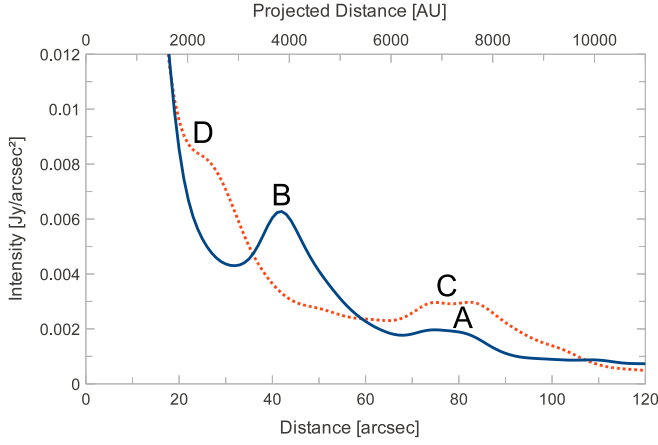


Fig. 2. Radial intensity profiles of Mira in the 70 μm band as a function of the distance to the star. Continuous (blue) line: integrated intensity across the arcs B and A ($75^\circ \leq PA \leq 180^\circ$). Dashed (red) line: across the arcs D and C ($190^\circ \leq PA \leq 270^\circ$). The top scale gives the distance from the star computed from Mira's distance of 91.7 pc.

3.2. Comparison with GALEX UV observations

Before drawing conclusions from the structures observed in the IR, it is interesting to confront these IR observations with GALEX ultraviolet observations of Mira in the far and near UV (152.8 nm and 227.1 nm, respectively; Martin et al. 2007). In the far UV image, Martin et al. (2007) found emission knots arranged north-west and south (Fig. 3). The axis of the streams is consistent with the direction of the bipolar outflow detected by Josselin et al. (2000), and moreover, the UV knots are exactly coincident with similar knots seen in $H\alpha$ (Meaburn et al. 2009). In contrast, Fig. 3 reveals that in the PACS 70 μm image the southern stream exactly corresponds to a region with an IR flux below the 3σ threshold¹. It thus looks as if the southern stream is penetrating and disrupting the material responsible for the IR emission. According to Meaburn et al. (2009), the southern stream is indeed inclined at an angle of 69° with respect to the plane of sky towards us. Put together, all these arguments clearly indicate that the IR emission must come from a 3D structure and is not confined to the orbital plane; otherwise, there could be no explanation for the anti-coincidence between the GALEX far UV/ $H\alpha$ emission and the IR emission.

Another interesting clue is that the northern lobe of the bipolar flow remains visible even though it is located behind the IR shell. The dust present in the shell will efficiently absorb the far UV radiation, so that the intensity of the northern lobe measured by GALEX should be smaller than that of the southern lobe, which has no intervening dust. In the far UV, the peak intensity of the northern lobe is indeed about 1.5 times fainter than the peak intensity of the southern lobe. Assuming that the northern and southern jets carry the same energy, this ratio may then be seen as resulting from dust extinction:

$$1/1.5 = \exp(-N\pi a^2 Q_{\text{ext,UV}}), \quad (1)$$

where N is the dust column density, a is the grain radius, and $Q_{\text{ext,UV}}$ is the ratio between the extinction cross section

¹ The 'hole' in the IR emission located about $1'$ to the East is less significant than the one considered, with fluxes about twice smaller for the latter.

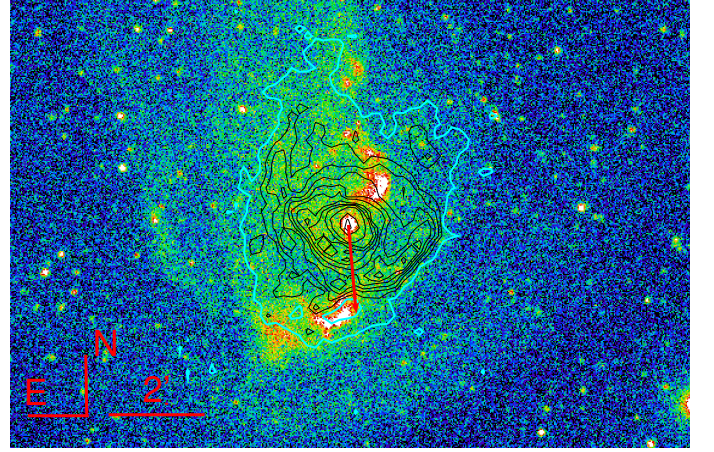


Fig. 3. GALEX far UV image of Mira obtained by Martin et al. (2007) overlaid with contours of the Herschel 70 μm image, the thick blue contour corresponding to an IR flux just 3σ above background. The bright white regions correspond to strong UV emission at both ends of the fast jet. Note the absence of IR emission at the end of the southern jet. The red arrow indicates the position of the star in 500 yrs. The bow shock is the faint structure in the background in the south-west.

and the geometrical section. This constraint can be inserted in Kirchhoff's law for the IR emission j_{IR} , leading to

$$j_{\text{IR}} = B_{\text{IR}}(T_{\text{dust}}) \ln(1.5) Q_{\text{abs,IR}}/Q_{\text{ext,UV}}, \quad (2)$$

where B_{IR} is the Planck intensity function at the dust temperature and $Q_{\text{abs,IR}}$ the ratio of the absorption cross section and the geometrical section. From Draine (1985), $Q_{\text{abs,70}\mu\text{m}}/Q_{\text{ext,0.15}\mu\text{m}} \sim 10^{-3}$ (almost independent of the grain size), which leads to

$$j_{\text{IR}} = 4.2 \times 10^{-4} B_{\text{IR}}(T_{\text{dust}}). \quad (3)$$

From the measured intensity ratio at 70 and 160 μm for the northern lobe, we find a dust temperature of 36 K; combining $B_{70\mu\text{m}}(36 \text{ K})$ with the measured $j_{70\mu\text{m}} = 4.42 \times 10^7 \text{ Jy/sr}$, we obtain $j_{70\mu\text{m}}/B_{70\mu\text{m}}(36 \text{ K}) = 1.2 \times 10^{-4}$, which agrees well with the value predicted by Eq. 3.

3.3. Role of the binary system

The arcs observed around Mira (Sect. 3.1) are (almost) unique in the MESS sample² (Groenewegen et al. 2011, Cox et al., in preparation), which makes it tempting to relate them to the binary nature of Mira.

In binary systems involving a mass-losing component, nested half-shells are seen when the orbit is orientated close to edge-on (He 2007), and they represent the 3D structure extending above the Archimedian spiral present in the plane of a circular orbit (for eccentric orbits, the spiral becomes broken). The latter was predicted by the hydrodynamics simulations of Theuns & Jorissen (1993), Mastrodemos & Morris (1999), Mohamed & Podsiadlowski (2011), and detected around

² The prototypical carbon star IRC +10216 is surrounded by a large number of thin and faint arcs, known for quite some time in the optical (Mauron & Huggins 1999, 2000), and now identified in Herschel images as well (Decin et al., in preparation). Their appearance is, however, quite different from the few thick arcs seen around Mira, in line with the fact that there is so far no evidence that IRC +10216 belongs to a binary system (Huggins et al. 2009).

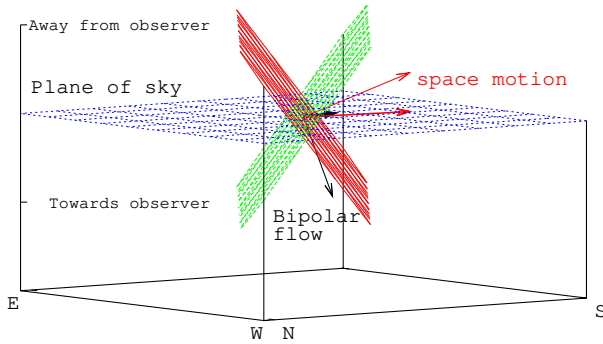


Fig. 4. Various vectors entering the discussion in a 3D view, with the red and green planes corresponding to the two possible orbital orientations. Because bipolar flows are generally perpendicular to the orbital plane, the green orientation seems the most likely. The sky plane is depicted in blue. The thick arrows are projections onto the sky plane. The observer is located on the bottom plane and looking upwards.

AFGL 3068 by Maunon & Huggins (2006) and Morris et al. (2006). In Mira, the observed arc structure resembles neither an Archimedian spiral, nor nested half-shells; its interpretation must therefore be more complex, involving two supplementary physical processes at play, namely the presence of a bipolar jet, and the interaction with the ISM (to fix the ideas, Fig. 4 presents the respective orientations of all relevant vectors involved in the Mira system). We already argued in Sect. 3.2 that the fast bipolar outflow (160 km s^{-1} ; Martin et al. 2007; Meaburn et al. 2009) seems to cut a hole in the IR shell (see Fig. 3). Similarly, it could easily disrupt the arcs with its high velocity, and may actually be responsible for cutting the edges of arcs B, C, and D, because all these edges are located along the southern jet, at a position angle close to 180° .

On the other hand, it is likely that the interaction with the ISM, more precisely, the termination shock, plays some role in shaping (at least) arc C, as already suggested by Ueta (2008) from lower-resolution *Spitzer* images, and confirmed in the *Herschel* images by the sharp ridge seen on the contour levels in Figs. 1c and 3. Arc C is indeed located almost upstream along Mira's space motion. On the $160 \mu\text{m}$ image (Fig. 1b), arcs A and C extend towards the north and join with each other, exactly opposite to the space motion of Mira, in a tail-like or bullet-like structure, as seen in the hydrodynamic simulations by Wareing et al. (2007) and Esquivel et al. (2010). This is clear evidence that the outer arcs feel the space motion and interact with the ISM. Another indication thereof is provided by the curvature of the bipolar-outflow southern stream, which Martin et al. (2007) attribute to its deceleration by the post-shock flow. Therefore, the arcs seen around Mira likely result from a combination of the projected 3D structures resulting from the interaction of Mira's wind with its companion on one hand, and with the ISM on the other hand.

As a first exploration of this combination, we used the simulations of Mohamed & Podsiadlowski (2007, 2011) of an AGB star nearly filling its Roche lobe in a system 10 AU -wide³, and losing mass through a slow wind. The 3D structure resulting from the expanding wind disturbed by the companion's gravi-

tational pull was then intersected with a paraboloid representing the bow shock. All particles within a thin shell along the paraboloid surface were kept and the resulting particle density projected onto the sky plane (the respective orientations of the paraboloid, the orbital plane, the sky plane, and the companion were taken into account, as represented in Fig. 4). If the IR emission observed by Herschel around Mira results from the reheating of the wind by the shock, this 'toy model', presented in Fig. 1d, should then give a fair account of the situation. Fig. 1d shows that there are indeed promising resemblances between the Herschel image and the one from the 'toy model', apart from the absence of brightening of the south-west arc C (where the compression from the ISM – not included in our model – is maximum), and apart from the ISM-swept appearance of the outermost northern arc. Hydrodynamical simulations of mass transfer in the Mira system, including the ISM interaction, are thus badly needed.

Acknowledgements. This work was supported in part by the Belgian Federal Science Policy Office via the PRODEX Programme of ESA (Nos. C90371 and C90372). AM and FK acknowledge funding by the Austrian Science Fund FWF under project number P23586-N16, RO under project number I163-N16. We thank A. Zijlstra and D. Pourbaix for discussions about Mira's orbit. SvE is FNRS Research Associate.

References

- Ardila, D. R. & Science Ground Segment Consortium, H. 2010, BAAS, 42, 397
- Draine, B. T. 1985, ApJS, 57, 587
- Esquivel, A., Raga, A. C., Cantó, J., et al. 2010, ApJ, 725, 1466
- Fong, D., Meixner, M., Sutton, E. C., Zalucha, A., & Welch, W. J. 2006, ApJ, 652, 1626
- Groenewegen, M. A. T., Waelkens, C., Barlow, M., et al. 2011, A&A, 526, A162
- He, J. H. 2007, A&A, 467, 1081
- Hevelius, J. 1662, Mercurius in Sole visus Gedani [...] Quibus accedit succincta Historiola, novæ illius, ac miræ stellæ in collo ceti, certis anni temporibus clare admodum affulgentis, rursus omnino evanescentis. [...] (Simon Reiniger, Danzig), p.146 sqq.
- Huggins, P. J., Maunon, N., & Wirth, E. A. 2009, MNRAS, 396, 1805
- Johnson, D. R. H. & Soderblom, D. R. 1987, AJ, 93, 864
- Josselin, E., Maunon, N., Planesas, P., & Bachiller, R. 2000, A&A, 362, 255
- Karovska, M., Hack, W., Raymond, J., & Guinan, E. 1997, ApJ, 482, L175
- Martin, D. C., Seibert, M., Neill, J. D., et al. 2007, Nature, 448, 780
- Mastrodemos, N. & Morris, M. 1999, ApJ, 523, 357
- Matthews, L. D., Libert, Y., Gérard, E., Le Bertre, T., & Reid, M. J. 2008, ApJ, 684, 603
- Maunon, N. & Caux, E. 1992, A&A, 265, 711
- Maunon, N. & Huggins, P. J. 1999, A&A, 349, 203
- Maunon, N. & Huggins, P. J. 2000, A&A, 359, 707
- Maunon, N. & Huggins, P. J. 2006, A&A, 452, 257
- Meaburn, J., López, J. A., Boumis, P., Lloyd, M., & Redman, M. P. 2009, A&A, 500, 827
- Mohamed, S. & Podsiadlowski, P. 2007, in ASP Conf. Ser. Vol. 372, ed. R. Napiwotzki & M. R. Burleigh, 15th European Workshop on White Dwarfs, 397
- Mohamed, S. & Podsiadlowski, P. 2011, in Asymmetric Planetary Nebulae V, ed. A. Zijlstra, F. Lykou, I. McDonald, & E. Lagadec (Jodrell Bank Centre for Astrophysics)
- Morris, M., Sahai, R., Matthews, K., et al. 2006, in IAU Symp., Vol. 234, Planetary Nebulae in our Galaxy and Beyond, ed. M. J. Barlow & R. H. Méndez, 469
- Ottensamer, R., Luntzer, A., Mecina, M., et al. 2011, in Why galaxies care about AGB stars (II) ?, ASP Conf. Ser., in press
- Poglitsch, A., Waelkens, C., Geis, N., et al. 2010, A&A, 518, L2
- Prieur, J. L., Aristidi, E., Lopez, B., et al. 2002, ApJS, 139, 249
- Raga, A. C. & Cantó, J. 2008, ApJ, 685, L141
- Reimers, D. & Cassatella, A. 1985, ApJ, 297, 275
- Roussel, H. 2011, A&A, submitted
- Schönrich, R., Binney, J., & Dehnen, W. 2010, MNRAS, 403, 1829
- Sokoloski, J. L. & Bildsten, L. 2010, ApJ, 723, 1188
- Theuns, T. & Jorissen, A. 1993, MNRAS, 265, 946
- Ueta, T. 2008, ApJ, 687, L33
- van Leeuwen, F. 2007, A&A, 474, 653
- Wareing, C. J., Zijlstra, A. A., O'Brien, T. J., & Seibert, M. 2007, ApJ, 670, L125

³ Although this separation is much smaller than the actual orbital separation of Mira system, this difference should not impact our conclusions, because the spiral properties are largely scale-invariant.